


Article

Effect of the Neck Linker on Processive Stepping of Kinesin Motor

Ping Xie 

Key Laboratory of Soft Matter Physics, Institute of Physics, Chinese Academy of Sciences, Beijing 100190, China; pxie@aphy.iphy.ac.cn

Abstract: Kinesin motor protein, which is composed of two catalytic domains connected together by a long coiled-coil stalk via two flexible neck linkers (NLs), can step processively on a microtubule towards the plus end by hydrolyzing adenosine triphosphate (ATP) molecules. To understand what the role is that the NL plays in the processive stepping, the dynamics of the kinesin motor are studied theoretically here by considering the mutation or deletion of an N-terminal cover strand that contributes to the docking of the NL in kinesin-1, the extension of the NL in kinesin-1, the mutation of the NL in kinesin-1, the swapping of the NL of kinesin-2 with that of kinesin-1, the joining of the stalk and neck of Ncd that moves towards the minus end of MT to the catalytic domain of kinesin-1, the replacement of catalytic domain of kinesin-1 with that of Ncd, and so on. The theoretical results give a consistent and quantitative explanation of various available experimental results about the effects of these mutations on motor dynamics and, moreover, provide predicted results. Additionally, the processive motility of kinesin-6 MKLP2 without NL docking is also explained. The available experimental data about the effect of NL mutations on the dynamics of the bi-directional kinesin-5 Cin8 are also explained. The studies are critically implicative to the mechanism of the stepping of the kinesin motor.

Keywords: molecular motor; kinesin; neck linker; mechanochemistry



Citation: Xie, P. Effect of the Neck Linker on Processive Stepping of Kinesin Motor. *Biophysica* **2023**, *3*, 46–68. <https://doi.org/10.3390/biophysica3010004>

Academic Editors: Ricardo L. Mancera, Paul C Whitford and Chandra Kothapalli

Received: 4 December 2022

Revised: 19 January 2023

Accepted: 23 January 2023

Published: 28 January 2023



Copyright: © 2023 by the author. Licensee MDPI, Basel, Switzerland. This article is an open access article distributed under the terms and conditions of the Creative Commons Attribution (CC BY) license (<https://creativecommons.org/licenses/by/4.0/>).

1. Introduction

Kinesin (typically kinesin-1 and kinesin-2) proteins are molecular motors that can move processively on microtubules (MTs) towards the plus end, which is powered by the hydrolysis of adenosine triphosphate (ATP) molecules [1]. A kinesin motor is composed of two N-terminal motor domains (also called heads) that are connected together by a long coiled-coil stalk via their two flexible neck linkers (NLs) [2,3]. The central and challenging issue for the kinesin motor is how the chemical energy of ATP hydrolysis is converted into the mechanical energy of the unidirectional movement, namely, the chemomechanical coupling mechanism [4–8]. For the purpose, a lot of structural, biochemical, and single molecule studies have been presented [9–16]. Meanwhile, various theoretical modeling and computational studies have been presented [17–24].

In the prevailing model presented in the literature, it was proposed that the docking of NL onto the head plays a critical role in the forward movement of the kinesin motor [25–30]. For convenience of writing, this model is called the NL-docking model here. To test the model, diverse experimental data have been provided on the dynamics of the kinesin motor via the mutation and/or deletion of the residues that are related to the NL [31–42]. Structural and atomistic molecular dynamics (AMD) studies showed that the NL docking is realized by the formation of a cover-neck bundle between an N-terminal cover strand and NL [31–33]. Thus, the single molecule experiments were performed about the influence of the mutation and/or deletion of the cover strand on the dynamics of kinesin-1 motor [34,35]. Puzzlingly, the experimental results showed that by deleting the cover strand, implying that the NL docking is nullified completely, the kinesin dimer can still move processively

towards the plus end with a velocity similar to the wild type (WT) case [34,35]. This is contrary to the inference derived from the NL-docking model. By extending the NL with the insertion of several residues near the C-terminus of the NL, it was found that the velocity of kinesin-1 was reduced largely relative to the WT case [36,37]. Case et al. [38] studied the velocity and ATPase rate of kinesin-1 motors by mutating some residues in the NL region and mutating some residues in the catalytic core which can interact with the NL. They found that the mutations greatly reduce the velocity, but the mutations have nearly no effect on the ATPase rate [38]. By designing the NL region to form a random coil, it was found that the mutant kinesin-1 motor also has a significant reduction of the velocity relative to the WT case, while the ATPase rate has only a very small reduction [38]. Andreasson et al. [39] found that while the kinesin-1 dimer with the NL being swapped with the NL of the kinesin-2 head can rarely move directionally on MTs, the kinesin-2 dimer with the NL being swapped with that of the kinesin-1 head behaves similar to the WT kinesin-2 dimer. Since the swapped NL cannot dock onto the head, it is thus implied that the NL docking plays little role in the forward movement of the kinesin-2 dimer, which is contradictory to the NL-docking model. By joining the stalk and neck of Ncd, which can move towards the minus end of an MT, to the motor domain of kinesin-1, the engineered motor can move towards the minus end of MT with a very small velocity compared to the WT kinesin-1 motor [40]. On the contrary, by replacing the catalytic domain of kinesin-1 with that of Ncd, the engineered motor can move towards the plus end with a velocity smaller than both the velocity of the WT kinesin-1 motor and that of the Ncd motor [41,42].

However, up to now a consistent and quantitative explanation of these diverse experimental data and, in particular, of those that are contrary to the NL-docking model has not been available. The purpose of this work is to address this issue, which is critical to the understanding of what the role is that the NL plays in the movement of the kinesin motors and thus is critically implicative to the chemomechanical coupling mechanism of the motors.

2. Methods

2.1. Model

To study theoretically the effect of NL on the dynamics of the kinesin motor, we use the same model for the chemomechanical coupling of the motor as that proposed before [43,44]. For the convenience of reading, the model is re-described here. We firstly present the main elements in the model, which are derived from the available biochemical, structural, and AMD simulation results.

- (i) The kinesin head in the nucleotide-free (ϕ), ATP, and ADP.Pi states has a high binding energy to MT [11,45,46], with the strong interaction between them inducing large conformational modulations of the local tubulin [47–49], while in adenosine diphosphate (ADP) state has a low binding energy to MTs [11,45,46], with the weak interaction between them inducing little conformational modulations of the tubulin [48,49]. The binding energy of the ADP-head to the tubulin with the large conformational modulations, which is denoted by E_{w1} , is much smaller than the binding energy of the ADP-head to the tubulin without the conformational modulations, which is denoted by E_{w2} [48,49]. This implies that after ATP transition to ADP, the head has a very weak binding energy E_{w1} to the local tubulin for a short time t_r (in the order of 10 μ s), and with the local tubulin returning elastically to the normally unmodulated one in time t_r , the binding energy of the ADP-head to the local tubulin transits to E_{w2} [48–50].
- (ii) The kinesin head in the ADP and ϕ states has an open nucleotide-binding pocket (NBP), while in the ATP and ADP.Pi states, it has a closed NBP and a large conformational change compared to that in the ADP/ ϕ states [51–53]. However, for the ATP- or ADP.Pi-head with its NL in the backward or minus-ended orientation (e.g., for the leading or plus-ended head of the dimer in the two-heads-bound state), the NBP closing and large conformational change are prohibited [53]. The head without the large conformational change has an undocked NL [53–56] and a high binding energy

- to the partner ADP-head [57], while the head with the large conformational change has a docked NL [53–56] and a very low binding energy to the partner ADP-head [57].
- (iii) The kinesin head with the NL in the forward or plus-ended orientation has a much larger rate of ATP transition to ADP than the head with the NL not in the forward orientation, as explained as follows. Structural studies indicated that the NL of the kinesin head in the forward orientation clashes with a nucleotide-binding motif (a P-loop subdomain) in the ϕ orientation, resulting in the P-loop subdomain in the ATP-like orientation [10]. Thus, it is expected that the rate of ATP transition to ADP of the head with the NL in the forward orientation is significantly increased compared to that with the NL not in the forward NL orientation. This is consistent with the prior biochemical data showing that the deletion of the NL in the kinesin-1 head and that in the kinesin-3/KIF1a head significantly reduced the ATPase rate but had no effect on the rate of ADP release [10,58].

The pathway for the chemomechanical coupling of the motor at saturating ATP is schematically shown in Figure 1. We begin with the minus-ended (trailing) and plus-ended (leading) heads in the ATP state binding strongly to tubulins II and III, respectively, on an MT filament (Figure 1a). The trailing head has the closed NBP, the docked NL, and the large conformational change compared to that in the ϕ state, while the leading head with the NL in the backward orientation has the open NBP and no conformational change. The trailing head has a much larger rate of ATP transition to ADP than the leading head.

First, in Figure 1a consider ATP transition to ADP in the trailing head (Figure 1b). The ADP-head has a very weak affinity E_{w1} to the local tubulin II within time t_r , during which the trailing head can (with a probability P_0) detach from tubulin II by overcoming E_{w1} and diffuse to the intermediate (INT) position relative to the MT-bound head, where the two heads have the high affinity (Figure 1c). Accordingly, within time t_r , the trailing head cannot (with probability $1-P_0$) detach from tubulin II and then the head binds to tubulin II with affinity E_{w2} until ADP release, followed by ATP binding (Figure 1a). In the INT state (Figure 1c), without the interference of the NL that is now not in the backward orientation, the large conformational change and NBP closing of the MT-bound ATP-head can take place rapidly, reducing greatly its affinity to the partner ADP-head and inducing its NL docking (Figure 1d). The detached ADP-head can then (with probability P_E) diffuse forward and bind to tubulin IV with affinity E_{w2} (Figure 1e), followed by ADP release and ATP binding (Figure 1f). From Figure 1d, the detached ADP-head can also (with probability $1-P_E$) diffuse backward and bind to tubulin II with affinity E_{w2} by overcoming the energy barrier (E_0) arising from both the NL undocking and the reverse large conformational change associated with the opening of the NBS of the leading ATP-head. Then, ADP is released from the trailing head, followed by ATP binding (Figure 1a). From Figure 1a to f, the dimer takes a forward step.

Second, in Figure 1a, consider ATP occasional transition to ADP in the leading head (Figure 1g). Within time t_r , the leading ADP-head can (with probability P_0) detach from the local tubulin III by overcoming E_{w1} and diffuse to the INT position (Figure 1h) and, accordingly, the leading ADP-head cannot (with probability $1-P_0$) detach from tubulin III until ADP release, followed by ATP binding (Figure 1a). From Figure 1h, the detached ADP-head can (with probability P_E) rebind to tubulin III with affinity E_{w2} in time t_r , followed by ADP release and ATP binding (Figure 1a). From Figure 1h, the detached ADP-head can also (with probability $1-P_E$) diffuse backward and bind to tubulin I with affinity E_{w2} by overcoming the energy barrier E_0 (Figure 1i), followed by ADP release and ATP binding (Figure 1j). From Figure 1a–j, the dimer takes a backward step.

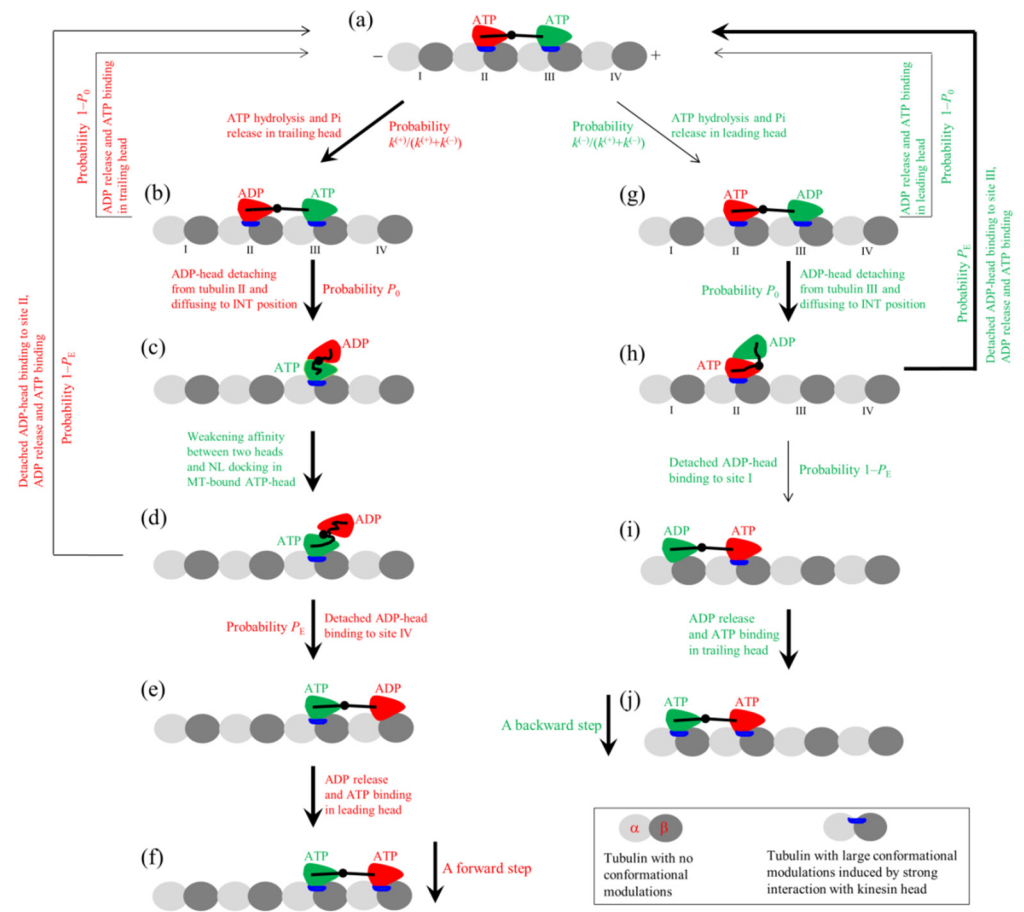


Figure 1. Model for processive stepping of the dimeric kinesin motor. (a–j) The chemomechanical coupling pathway at saturating adenosine triphosphate (ATP) concentrations. At saturating ATP, the nucleotide-free state of the kinesin head is so short that it is not needed to be considered. Since in both the ATP and ADP.Pi states, the kinesin head has a similar conformation and has a high affinity to an MT, for simplicity, ATP hydrolysis and Pi release are treated as one step in the ATP transition to adenosine diphosphate (ADP). The thickness of an arrow indicates the relative magnitude of the probability of the transition between two states connected by the arrow for the WT kinesin motor under no load.

2.2. General Equations for Motor Dynamics

In this section, on the basis of the pathway (Figure 1), we present equations for the dynamics of the kinesin motor. Let $k^{(+)}$ and $k^{(-)}$ represent the rate of ATP transition to ADP of the trailing head with the forward NL orientation and that of the leading head without the forward NL orientation, respectively, and k_D represent the rate of ADP release from the MT-bound ADP-head (for simplicity, k_D is treated as independent of the NL orientation). As discussed before [43,44], these rates are independent of the force on the NL, which is consistent with the available experimental data [28,59–61]. Considering that at the INT state, the NL docking of the MT-bound ATP-head takes place with a rate being much larger than $k^{(+)}$ and $k^{(-)}$ [62], the overall ATPase rates of the trailing and leading heads can be written as [44]:

$$k_T = \frac{k^{(+)}k_D}{k^{(+)} + k_D} (1 - P_0) + k^{(+)}P_0P_E + \frac{k^{(+)}k_D}{k^{(+)} + k_D} P_0(1 - P_E), \tag{1}$$

$$k_L = \frac{k^{(-)}k_D}{k^{(-)} + k_D} (1 - P_0) + \frac{k^{(-)}k_D}{k^{(-)} + k_D} P_0P_E + k^{(-)}P_0(1 - P_E), \tag{2}$$

where P_0 and P_E are dependent on the load acting on the motor. Here, we define the backward load as having a negative value (with $F < 0$) and the forward load as having a positive value (with $F > 0$). For $F < 0$, after ATP transition to ADP in the trailing head, P_0 is approximately independent of F on the coiled-coil stalk, and after ATP transition to ADP in the leading head, the load dependence of P_0 has the form [44]:

$$P_0 = 1 - \left(1 - P_0^{(0)}\right) \exp\left(-\frac{|F|}{F_0}\right), \quad (3)$$

where $P_0^{(0)}$ is P_0 under $F = 0$ and F_0 is the characteristic force for the head to escape from the potential well of depth E_{w1} and diffuse to the INT position. For $F > 0$, after ATP transition to ADP in the leading head, P_0 is approximately independent of F , and after ATP transition to ADP in the trailing head, the load dependence of P_0 has the form of Equation (3) [44]. The load dependence of P_E for both $F < 0$ and $F > 0$ has the form [44,63]:

$$P_E = \frac{\exp(\beta E_0) \exp(\beta F \delta)}{\exp(\beta E_0) \exp(\beta F \delta) + 1}, \quad (4)$$

where $E_0 = E_C + E_{NL}$, with E_C and E_{NL} being the free energy change associated with the large conformational change of the head induced by ATP binding and that associated with the NL docking, respectively, $\beta^{-1} = k_B T$ is the Boltzmann constant times the absolute temperature, and δ is the force-sensitivity distance that depends on the MT-binding surface of ADP-head or the potential form of ADP-head interacting with the MT. The total ATPase rate k and velocity v of the motor can be written as:

$$k = k_T + k_L, \quad (5)$$

$$v = [P_0 P_E k_T - P_0 (1 - P_E) k_L] d, \quad (6)$$

where $d = 8.2$ nm is the repeat period of tubulins in an MT filament. The number of ATP molecules consumed per forward step can be written as:

$$N = \frac{k_T + k_L}{P_0 P_E k_T}. \quad (7)$$

3. Results

3.1. Dynamics of Kinesin-1 with Mutation or Deletion of Cover Strand Contributing to NL Docking

Prior studies showed that NL docking is realized by the formation of the cover-neck bundle between the N-terminal cover strand and NL [31–33]. Thus, the mutation of the cover strand will weaken the NL docking and the deletion of the cover strand will nullify the NL docking. However, the experimental data showed that by mutating or deleting the cover strand, the kinesin dimer can still move processively towards the plus end even with the unloaded velocity slightly larger than the WT case [34,35]. In this section, we study theoretically the effect of the mutation or deletion of the cover strand on the velocity of kinesin-1, explaining quantitatively the puzzling experimental data [34,35]. For kinesin-1, with its NLs having the native length, due to the large internal force in the two-heads-bound state [64], after one head transiting from ATP state to ADP state, the head can easily detach from the local tubulin by overcoming the very weak E_{w1} and then diffuse to the INT position. Thus, for approximation, we take $P_0 = 1$ for the case studied in this section.

From the equations presented in Section 2.2, it is seen that to calculate the velocity, values of parameters k_D , $k^{(+)}$, $k^{(-)}$, E_0 and δ are required for the case of $P_0 = 1$. From the prior biochemical data showing that the rate constant of ADP release from the MT-bound head is about 250 s^{-1} [59], we take $k_D = 250 \text{ s}^{-1}$ here and throughout (Table 1). From the prior biochemical data showing that the deletion of the NL in the kinesin-1 head significantly reduced the ATPase rate [10], we take $k^{(-)} = 0.01 k^{(+)}$ for the *Drosophila melanogaster* kinesin-1

(Table 1). Then, by adjusting the values of the other three parameters $k^{(+)}$, E_0 , and δ (Table 1) the single-molecule data of the velocity versus the backward load for the WT motor, the mutant one with two mutated residues A9G and S12G in the cover strand (called 2G), and the mutant one with deletion of the entire cover strand (called DEL) measured by Khalil et al. [34] can be reproduced well (Figure 2). The sensitivity of the theoretical results to the variation of the adjustable parameter value is studied, which shows that the small variation of the parameter value has only a small effect on the theoretical results, indicating that the results are robust. Moreover, from Figure 2, it is noted that under no load the velocity of the 2G and that of the DEL are increased by about 1.12-fold relative to that of the WT, which is also consistent with the experimental data of Budaitis et al. [35] showing that the unloaded velocity of the cover-neck-bundle mutant is increased by about 1.25-fold relative to that of the WT.

Table 1. Parameter values for *Drosophila melanogaster* kinesin-1 motors.

Parameter	Value		
	WT	2G	DEL
k_D (s ⁻¹)	250	250	250
$k^{(+)}$ (s ⁻¹)	62 *	72 *	79 *
$k^{(-)}$	$0.01k^{(+)}$	$0.01k^{(+)}$	$0.01k^{(+)}$
E_0 ($k_B T$)	4.8 *	3.3 *	2.1 *
δ (nm)	4.7 *	5.5 *	7.9 *

Values with “*” are obtained by fitting to the single molecule data of Khalil et al. [34], while values of other parameters are kept fixed.

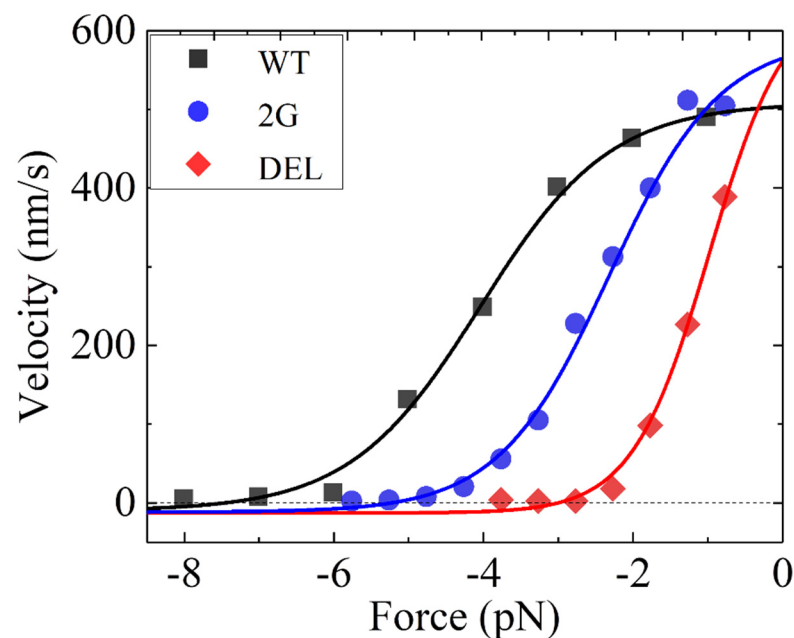


Figure 2. Dependence of velocity on backward load for *Drosophila melanogaster* kinesin-1 motors. WT, 2G, and DEL represent the wild type, the mutant 2G with two residues A9G and S12G in the cover strand, and the mutant DEL lacking the entire cover strand, respectively. Lines are theoretical results. Symbols are experimental data taken from Khalil et al. [34].

From Table 1, it is seen that the values of $k^{(+)}$ and $k^{(-)}$ for the 2G and DEL are slightly larger than those of the WT, implying that the mutation or deletion of the cover strand slightly enhances the rate of ATP transition to ADP. From Table 1, it is seen that E_0 for the DEL is smaller by $2.7k_B T$ than that for the WT. Considering that no NL docking can

occur for the DEL, this implies that the NL-docking energy of the WT is $E_{NL} = 2.7k_B T$ and, accordingly, the free energy change of the large conformational change of the head induced by ATP binding is $E_C = E_0 - E_{NL} = 2.1k_B T$, implying that E_C and E_{NL} have the similar values. The above value of $E_{NL} = 2.7k_B T$ is consistent with the prior biochemical data of a few $k_B T$ [65] and that of $E_C = 2.1k_B T$ is also consistent with the prior AMD simulated data of a few $k_B T$ [66]. Moreover, E_0 for the 2G is smaller by $1.5k_B T$ than that for the WT, implying that for the 2G, the NL-docking energy is about $2.7k_B T - 1.5k_B T = 1.2k_B T$. From Table 1, it is seen that δ for the 2G and for the DEL are different from that for the WT. Based on our model, this implies that the mutation or deletion of the cover strand affects the potential form of the interaction of the head in the ADP state with an MT. This is consistent with the experimental data of Budaitis et al. [35] showing that the mutations of the cover strand affect the landing rate of the motor, which arises from the change in the MT-binding surface of the ADP-head or the potential form of the ADP-head interacting with an MT. Since the mutation or deletion of the cover strand induces the change in the potential form of the ADP-head interacting with the MT, it is expected that the 2G and DEL would have different force-sensitivity distances from the WT for the dissociation in the weakly MT-binding (ADP) state. The cover-neck-bundle mutant has a higher landing rate than the WT [35], implying that the former has a larger MT-binding surface than the latter. Thus, the 2G and DEL would have larger force-sensitivity distances than the WT, resulting in the 2G and DEL dissociating from the MT at lower forces than the WT (see, e.g., analyses in Ref. [44]), consistent with the available experimental data [34,35].

3.2. Dynamics of Kinesin-1 with NL Extension

In this section, we study the effect of the extension of the NL on the velocity of human kinesin-1. One purpose of this study is to determine the parameter values for the human kinesin-1, which will be used in later studies. As mentioned in the above section, for the WT case, the large internal force results in $P_0 \approx 1$. However, for the mutant case with the NL in each head being extended by six residues (e.g., AEQKLT) at its C-terminus (with the mutant motor being called 6AA), as done in the experiments of Andreasson et al. [36,37], the internal force becomes nearly zero when two heads are bound to the MT, thus resulting in $P_0^{(0)} < 1$, as prior Brownian dynamics simulations showed [64].

From the equations presented in Section 2.2, it is seen that to calculate the velocity, values of parameters k_D , $k^{(+)}$, $k^{(-)}$, E_0 , δ , $P_0^{(0)}$, and F_0 are required. Since the extended residues are at the C-terminus of the NL, they have little effect on the ATPase activity, the conformational change of the head, NL docking, and the interaction of the head with the MT. Thus, both the WT and 6AA should have the same values for k_D , $k^{(+)}$, $k^{(-)}$, E_0 , and δ . For the WT, $P_0 = 1$, and thus no parameter F_0 is needed. We still take $k_D = 250 \text{ s}^{-1}$ for the human kinesin-1 (Table 2). We take $k^{(-)} = 0.15k^{(+)}$ for the human kinesin-1 (Table 2). Then, by adjusting values of the other five parameters $k^{(+)}$, E_0 , δ , $P_0^{(0)}$, and F_0 (Table 2), the single molecule data of the velocity versus both the backward and forward loads for both the WT and 6AA measured by Andreasson et al. [37] can be reproduced well (Figure 3). The studies of the sensitivity of the theoretical results to the variation in the adjustable parameter value show that the results are robust (data not shown). Moreover, with the parameter values given in Table 2, under no load, the number of ATP molecules consumed per forward step is $N = 1.16$ for the WT and $N = 3.2$ for the 6AA. This value of $N = 1.16$ for the WT gives the chemomechanical coupling efficiency of about 0.86, which is close to the experimental value of about 0.81 for the WT human kinesin-1 measured by Yildiz et al. [61]. The value of $N = 3.2$ for the 6AA is close to the experimental data of about 3.5 for the human 6AA kinesin-1 measured by Clancy et al. [36]. Thus, both the theoretical and experimental results indicate that even under no load the 6AA behaves evidently as a non-tight chemomechanical coupling motor, as studied before for the WT kinesin-1 motors under the backward load [67].

Table 2. Parameter values for human kinesin-1 motors.

Parameter	Value
k_D (s^{-1})	250
$k^{(+)}$ (s^{-1})	92 *
$k^{(-)}$	$0.15k^{(+)}$
E_0 ($k_B T$)	4.5 *
δ (nm)	4.2 *
F_0 (pN)	3.8 *
$P_0^{(0)}$	1 (for K1-WT) 0.37 * (for K1-6AA)

Values of parameters with "*" are obtained by fitting to the single molecule data of Andreasson et al. [37], while values of other parameters are kept fixed.

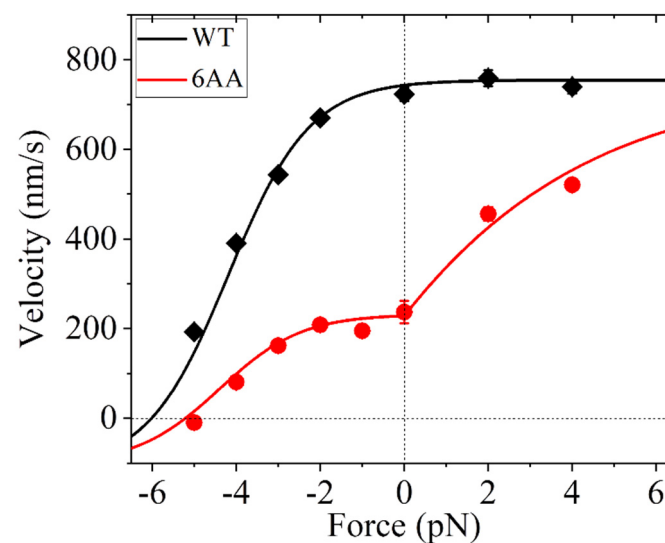


Figure 3. Dependence of velocity on backward and forward loads for human kinesin-1 motors. WT and 6AA represent the wild type and the mutant one with extension of each NL by inserting six additional residues AEQKLT, respectively. Lines are theoretical results. Symbols are experimental data taken from Andreasson et al. [37].

Comparing parameter values of Table 2 with those of Table 1, it is seen that $E_0 = 4.5k_B T$ for the human kinesin-1 is close to $E_0 = 4.8k_B T$ for the *Drosophila melanogaster* kinesin-1, and $\delta = 4.2$ nm for the human kinesin-1 is also close to $\delta = 4.7$ nm for the *Drosophila melanogaster* kinesin-1.

3.3. Dynamics of Kinesin-1 with NL Mutation

In this section, we study the effects of the mutation of the NL region and the mutation of some residues in the catalytic core, which can interact with the NL region, on the dynamics of human kinesin-1, explaining quantitatively the experimental data measured by Case et al. [38].

First, consider alanine substitutions of two conserved glycines in loop 13 of the catalytic core, Gly291 and Gly292, which can interact with the NL region, as performed in the experiments of Case et al. [38]. The mutant motor is called K1-G291A/G292A here. Since Gly291 and Gly292 could be important for allowing motion within the motor domain, as mentioned in Case et al. [38], it is reasonably argued that the two residues affect the conformational change of the head after its transition from the ATP to the ADP state, which can be tested using future molecular dynamics simulations such as using the structure-based coarse-grained modeling [68,69]. Thus, the conformation of the head in the ADP state in the K1-G291A/G292A would have a conformation slightly different from that in the WT,

resulting in the ADP-head in the K1-G291A/G292A having E_{w1} evidently larger than that in the WT. Hence, it is expected that $P_0^{(0)}$ is much smaller than 1 for the K1-G291A/G292A.

Second, consider alanine substitutions of Ile325, Lys326, and Asn327 in the NL, as performed in the experiments of Case et al. [38]. The mutant motor is called K1-I325A/K326A/N327A here. Since Gly292 interacts with residue Asn327 of the NL, as mentioned in Case et al. [38], it is reasonably argued that Asn327 can also affect the conformational change of the head after its transition from the ATP to ADP state and, thus, the conformation of the ADP-head in the K1-I325A/K326A/N327A has a conformation slightly different from that in the WT, resulting in the ADP-head in the K1-I325A/K326A/N327A having E_{w1} evidently larger than that in the WT (the consistency of this argument with the biochemical data will be discussed at the end of this section). Thus, it is expected that $P_0^{(0)}$ for the K1-I325A/K326A/N327A is smaller than 1. Since the effect of Asn327 is via its interaction with Gly292, it is expected that $P_0^{(0)}$ for the K1-I325A/K326A/N327A should be larger than that for the K1-G291A/G292A.

From the equations presented in Section 2.2, it is seen that to calculate the velocity and ATPase rate, values of parameters k_D , $k^{(+)}$, $k^{(-)}$, $E_0 = E_C + E_{NL}$, δ , $P_0^{(0)}$, and F_0 are required. As mentioned above, $P_0^{(0)}$ has a value for the K1-G291A/G292A that is different from that for the K1-I325A/K326A/N327A. For the WT, we have $P_0^{(0)} = 1$ (see above). Moreover, it is evident that E_{NL} has a value for the K1-G291A/G292A that is different from that for the K1-I325A/K326A/N327A and from that for the WT. Thus, the WT, K1-G291A/G292A, and K1-I325A/K326A/N327A have different values of E_0 . Here, we take the values of $P_0^{(0)}$ and E_{NL} to be variable. In the model, the mutations in the K1-G291A/G292A have little effect on the ATPase activity, as explained as follows. The mutated residue can still clash with the P-loop subdomain in the ϕ orientation, with the P-loop subdomain in the ATP-like orientation, and thus the mutations would have a slight effect on the ATPase activity. Consequently, we take the same values of k_D , $k^{(+)}$, and $k^{(-)}$ for the WT, K1-G291A/G292A, and K1-I325A/K326A/N327A, as given in Table 2. In addition, we take the same values of δ and F_0 for the WT, K1-G291A/G292A, and K1-I325A/K326A/N327A, as given in Table 2. Under no load, the theoretical results of the velocity and total ATPase rate versus $P_0^{(0)}$ for different values of E_0 are shown in Figure 4a,b, respectively, where the velocity and ATPase rate at $P_0^{(0)} = 1$ and $E_0 = 4.5k_B T$ correspond to the WT case. From Figure 4a,b, it is seen that for the value of E_0 in the range from $4.5k_B T$ to $1.5k_B T$, which correspond to E_{NL} for the WT in the range from 0 to $3k_B T$, the curves of velocity and ATPase rate versus $P_0^{(0)}$ change only slightly. As determined in Figure 2, $E_{NL} = 2.7k_B T$ for the *Drosophila melanogaster* kinesin-1. Thus, the results shown in Figure 4a,b imply that the variation in E_{NL} arising from the mutations in the K1-G291A/G292A and K1-I325A/K326A/N327A has only a slight effect on the velocity and ATPase rate. Moreover, from Figure 4a,b, it is seen interestingly that at $P_0^{(0)} = 1, 0.12,$ and 0.01 , the theoretical results of both the velocity and ATPase rate are in quantitative agreement with the experimental data for the WT, K1-I325A/K326A/N327A, and K1-G291A/G292A, respectively, as measured by Case et al. [38]. This thus implies that $P_0^{(0)} = 0.12$ for the K1-I325A/K326A/N327A and $P_0^{(0)} = 0.01$ for the K1-G291A/G292A, with the latter being much smaller than the former, which is consistent with the discussion mentioned above.

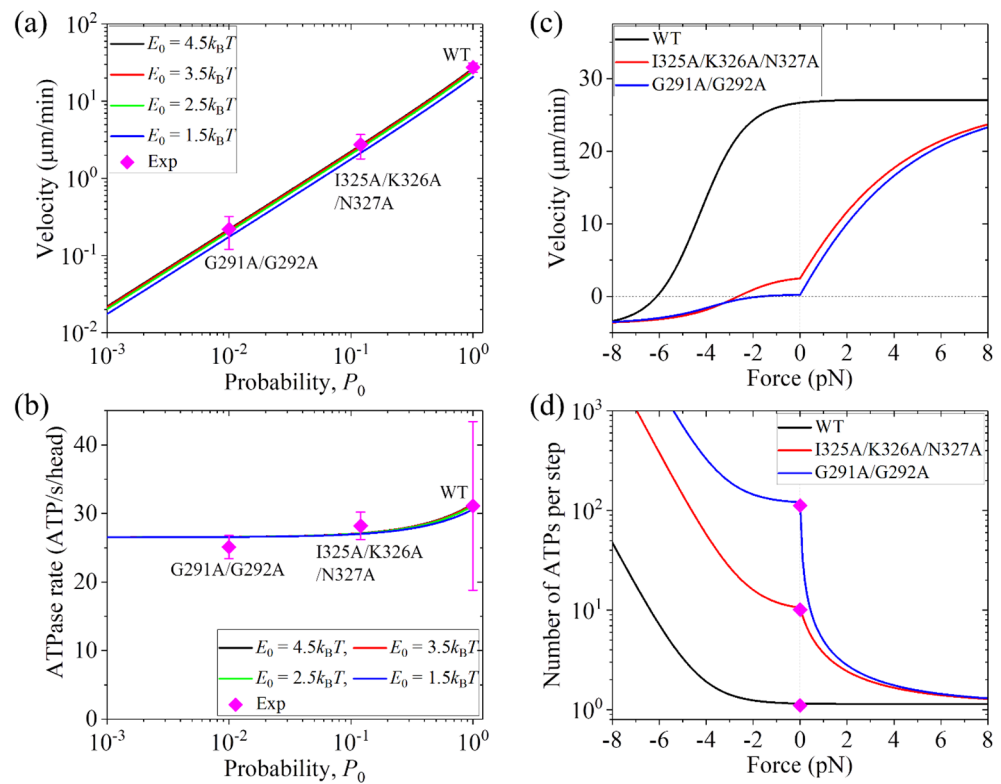


Figure 4. Dynamics of human kinesin-1 motors. WT, I325A/K326A/N327A, and G291A/G292A represent the wild type K560, the mutant K560-I325A/K326A/N327A with Ile325, Lys326, and Asn327 in NL being changed to alanine and the mutant K560-G291A/G292A with Gly291 and Gly292 in loop 13 of the catalytic core being changed to alanine, respectively. Lines are theoretical results. Symbols are experimental data taken from Case et al. [38]. (a) Velocity versus probability P_0 under no load for different values of E_0 . Note that the red line is almost coincident with the black line and thus the red line cannot be discerned. (b) ATPase rate per head versus probability P_0 under no load for different values of E_0 . Note that the red line is almost coincident with the black line and thus the red line cannot be discerned. (c) Velocity versus backward and forward loads. Data for the WT, I325A/K326A/N327A, and G291A/G292A are calculated with E_0 listed in Table 2 being subtracted by $E_{NL} = 0, 2k_B T$, and $1k_B T$, respectively. (d) Number of ATPs consumer per step versus backward and forward loads. Data for the WT, I325A/K326A/N327A, and G291A/G292A are calculated with E_0 listed in Table 2 being subtracted by $E_{NL} = 0, 2k_B T$, and $1k_B T$, respectively. The experimental data are calculated with $N = 2k_{cat}d/v$ ($d = 8.2$ nm), where k_{cat} is the ATPase rate per head and v is the velocity measured by Case et al. [38].

Furthermore, we provide predicted results on the load dependences of velocity and number of ATPs per step for the WT, K1-I325A/K326A/N327A, and K1-G291A/G292A. As determined just above, $P_0^{(0)} = 1, 0.12$, and 0.01 for the WT, K1-I325A/K326A/N327A, and K1-G291A/G292A, respectively. As given in Table 2, $E_0 = 4.5k_B T$ for the WT. Since the mutations in the K1-I325A/K326A/N327A have a direct effect on the NL docking, we take $E_0 = 2.5k_B T$ for the K1-I325A/K326A/N327A, equivalent to E_{NL} being reduced by $2k_B T$ relative to the WT case. Since the mutations in the K1-G291A/G292A have an indirect effect on the NL docking, we take $E_0 = 3.5k_B T$ for the K1-G291A/G292A, equivalent to E_{NL} being reduced by $1k_B T$ relative to the WT case. The values of other parameters are from Table 2. In Figure 4c,d, we show the theoretical results on the load dependences of velocity and number of ATPs per step for the three motors. From Figure 4c, it is seen interestingly that with the increase in the forward load, while the velocity for the WT is kept nearly unchanged, the velocities for the K1-I325A/K326A/N327A and K1-G291A/G292A increase significantly and level out to the WT case at the high forward load. From Figure 4d, it is

seen interestingly that under no load, the numbers of ATPs per step are about 1.16, 10.58, and 121.23 for the WT, K1-I325A/K326A/N327A, and K1-G291A/G292A, respectively, which are in good agreement with the experimental data measured by Case et al. [38]. This indicates that even under no load, the K1-I325A/K326A/N327A and K1-G291A/G292A behave evidently as non-tight chemomechanical coupling, similar to the 6AA motor studied in the above section. With the increase in the forward load, while the number of ATPs per step for the WT is kept nearly to one, the numbers for the K1-I325A/K326A/N327A and K1-G291A/G292A decrease significantly and level out to the WT case at the high forward load. These predicted results shown in Figure 4c,d can be tested using future single-molecule optical trapping experiments.

In addition, consider residues 323–332 in the NL region being designed to form a random coil termed ran10, as performed in the experiments of Case et al. [38]. The mutant motor is called K1-ran10 here. Since some of these mutated residues could interact with the residues in the motor domain which are important for allowing motion within the motor domain, it is thus expected that $P_0^{(0)}$ for the K1-ran10 should also be very small, resulting in a very small velocity of the K1-ran10, thus explaining the experimental data of Case et al. [38]. It is noted that the argument for the ADP-head of the K1-ran10 having a larger affinity for the MT than the WT ADP-head is supported by the biochemical data of Case et al. [38] showing that the K1-ran17, where residues 323–339 are designed to be random ones, in the presence of 1 mM ADP exhibited about 3-fold higher MT affinity (with an equilibrium dissociation constant $K_D = 6.9 \pm 0.4 \mu\text{M}$) than the corresponding WT protein (with $K_D = 21.1 \pm 3.4 \mu\text{M}$). The argument is also consistent with the experimental data showing that a single K1-ran17 in the monomeric form exhibits a motility that is much (about 200-fold) smaller than a single WT in the monomeric form [38].

3.4. Dynamics of Kinesin-2 with NL Swapping

The experimental data of Andreasson et al. [39] showed that while the kinesin-1 dimer with the NL in each head being swapped with that of the kinesin-2 KIF3A head can rarely move directionally on an MT, the kinesin-2 KIF3AB dimer with the NL in each head being swapped with that of the kinesin-1 head behaves similar to the KIF3AB dimer. The latter mutant dimer is simply called K2-KHC dimer here. The above experimental data for the kinesin-1 dimer with each head having the NL of the KIF3A head can be readily explained with the studies shown in the above section for the K1-ran10. In this section, we explain the experimental data for the K2-KHC dimer.

Since the NL-orientation-dependent ATPase activity is due to the clash of the P-loop subdomain in the ϕ orientation with the residues in the NL of the forward orientation [10], it is thus expected that the swapping of the NL of the kinesin-2 head with that of the kinesin-1 head has little effect on the ATPase activity of the kinesin-2 head, similar to the case for the kinesin-1 head (see above section). However, different from the case for the kinesin-1 head, for the case of the kinesin-2 head, it is argued that the residues in the catalytic core, which can interact with those in the NL, have little effect on the conformational change of the head after its transition from the ATP to ADP state, with both the WT kinesin-2 head in the ADP state having the similar weak affinity to tubulin as the kinesin-2 head with the kinesin-1 NL. This argument can be easily tested by biochemically measuring the equilibrium dissociation constant of the kinesin-2 head with the kinesin-1 NL from the MT and comparing it with that of the WT kinesin-2 head in the presence of saturating ADP, as performed in Case et al. [38] for the K1-ran17 and the corresponding WT protein (see above section). As previous studies showed, due to the NL in each head of the KIF3AB dimer having a longer length than that in the kinesin-1 head, while $P_0^{(0)} = 1$ for the kinesin-1 dimer, $P_0^{(0)} < 1$ for the KIF3AB dimer [44]. Here, for the K2-KHC dimer, we consider two cases. One case is that the K2-KHC dimer has the same value of $P_0^{(0)}$ as that for the KIF3AB dimer, while the other case is that, due to the shorter NLs in the K2-KHC dimer than in the

KIF3AB dimer, $P_0^{(0)} = 1$ for the K2-KHC dimer, as in the case of the kinesin-1 dimer. For convenience, the former case is called K2-KHC-1 and the latter case is called K2-KHC-2.

As in the above section for the human kinesin-1, we still take $k_D = 250 \text{ s}^{-1}$ and $k^{(-)} = 0.15k^{(+)}$ for the KIF3AB and K2-KHC dimers (Table 3). Then, by adjusting values of the other five parameters $k^{(+)}$, E_0 , δ , $P_0^{(0)}$, and F_0 (Table 3), the single-molecule data of the velocity versus both the backward and forward loads for the KIF3AB dimer (WT) measured by Andreasson et al. [39] can be reproduced well (Figure 5). The studies of the sensitivity of the theoretical results to the variation of the adjustable parameter value show that the results are robust (data not shown). For the K2-KHC dimer, we take E_0 to be half of that for the WT (Table 3), equivalent to E_C and E_{NL} having the same value for the WT. With the parameter values given in Table 3, the theoretical results on the load dependence of velocity for the K2-KHC-1 and for the K2-KHC-2 are also shown in Figure 5. It is seen that under a forward load or no load, the WT, K2-KHC-1, and K2-KHC-2 show similar velocities, which is consistent with the experimental data of Andreasson et al. [39]. The prominent difference between the WT and K2-KHC-1 or K2-KHC-2 is that the latter has a smaller stall force than the former, which can be easily tested using future single-molecule optical trapping experiments.

Table 3. Parameter values for kinesin-2 KIF3AB motors.

Parameter	Value
$k_D \text{ (s}^{-1}\text{)}$	250
$k^{(+)} \text{ (s}^{-1}\text{)}$	88.5 *
$k^{(-)}$	$0.15k^{(+)}$
$E_0 \text{ (k}_B T\text{)}$	3.05^* (for WT) $3.05/2$ (for K2-KHC-1 and K2-KHC-2)
$\delta \text{ (nm)}$	2^*
$F_0 \text{ (pN)}$	4.5^*
$P_0^{(0)}$	0.82 (for WT) * 0.82 (for K2-KHC-1) 1 (for K2-KHC-2)

Values of parameters with "*" are obtained by fitting to the single molecule data of Andreasson et al. [39] for the WT, while values of other parameters are kept fixed.

3.5. Dynamics of Motor with Ncd Stalk and Neck Joined to the Kinesin-1 Motor Domain

In this section, we consider the engineered motor consisting of the Ncd stalk and neck joined to the motor domain of kinesin-1, as performed in the experiments of Endow and Waligora [40]. The engineered motor is called the NcdKHC motor here. For the NcdKHC head in the ATP and ADP states, its neck region tilts towards the minus- and plus-ended directions, respectively, as for the WT Ncd determined structurally before [70]. Thus, from the pathway of Figure 1, it is inferred that the pathway for the NcdKHC dimer can be schematically shown in Figure 6, where for approximation, we take $P_0 = 1$, as for the WT kinesin-1 dimer.

We still begin the pathway with the minus-ended head in the ATP state binding strongly to tubulin II and the plus-ended head in the ATP state binding strongly to tubulin III (Figure 6a). The minus-ended head with the forward NL orientation has a much larger rate of ATP transition to ADP than the plus-ended head without the forward NL orientation (see Section 2.1). First, consider ATP transition to ADP in the minus-ended head (Figure 6b). The head then detaches easily from tubulin II by overcoming E_{w1} and diffuses to the INT position (Figure 6c). In the INT state, the neck region of the MT-bound ATP-head tilts towards the minus-ended direction. The large conformational change of the MT-bound ATP-head greatly reduces the affinity between the two heads. Then, with probability P_E , the detached ADP-head can diffuse in the plus-ended (forward) direction and bind to tubulin IV by overcoming the total free energy (E_{NL}) of retaining the neck region of the minus-ended ATP-head tilting towards the minus-ended direction and of retaining the neck region

of the plus-ended ADP-head tilting towards the plus-ended direction (Figure 6d). Then, ADP is released from and ATP binds to the plus-ended head (Figure 6e). Alternatively, with probability $1-P_E$, the detached ADP-head can diffuse in the minus-ended (backward) direction and bind to tubulin II by overcoming the free energy change associated with the large conformational change of the plus-ended ATP-head, followed by ADP release and then ATP binding in the new minus-ended head (Figure 6a). From Figure 6a–e, a forward step of the motor was made by hydrolyzing one ATP.

Second, in Figure 6a, consider ATP transition to ADP in the plus-ended head (Figure 6f). The head detaches easily from tubulin III by overcoming E_{w1} and diffuses to the INT position (Figure 6g). Then, with probability P_E , the detached ADP-head can diffuse in the plus-ended (forward) direction and bind to tubulin IV in time t_r by overcoming the free energy E_{NL} (see just above), followed by ADP release and then ATP binding (Figure 6a). Alternatively, with probability $1-P_E$, the detached ADP-head can diffuse in the minus-ended (backward) direction and bind to tubulin I by overcoming the free energy change associated with the large conformational change of the plus-ended ATP-head (Figure 6h). Then, ADP is released from and ATP binds to the minus-ended head (Figure 6i). From Figure 6a–i, a backward step of the motor was made by hydrolyzing one ATP.

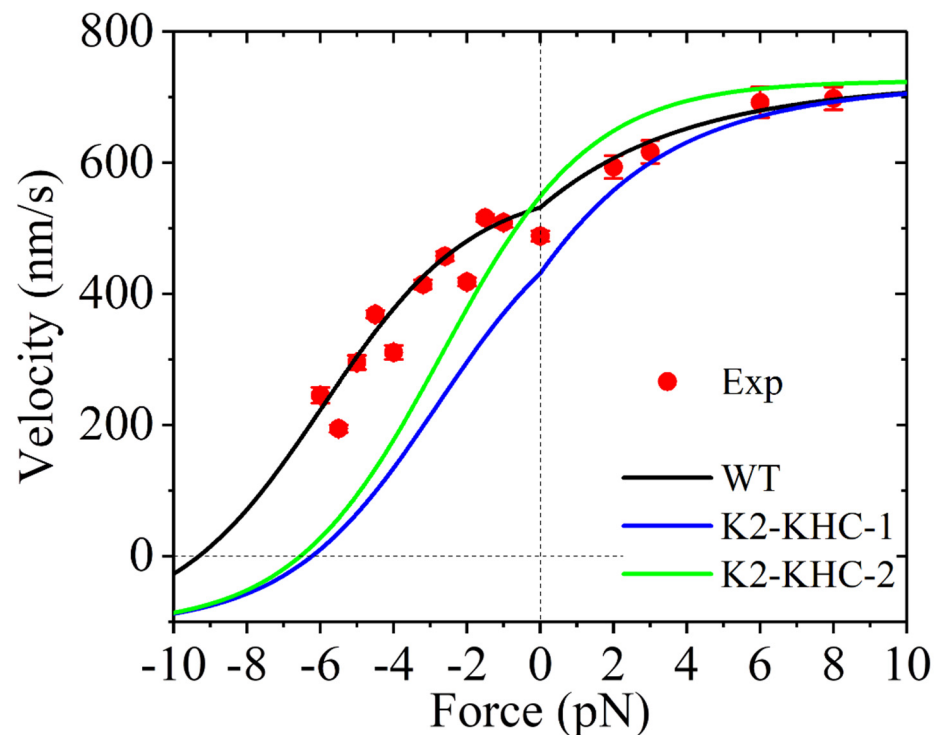


Figure 5. Dependence of velocity on backward and forward loads for mammalian kinesin-2 KIF3AB motors. Lines are theoretical results. Symbols are experimental data taken from Andreasson et al. [39]. WT and K2-KHC represent the wild type and the mutant one with its NL in each head being swapped with that of *Drosophila* kinesin-1 head, respectively.

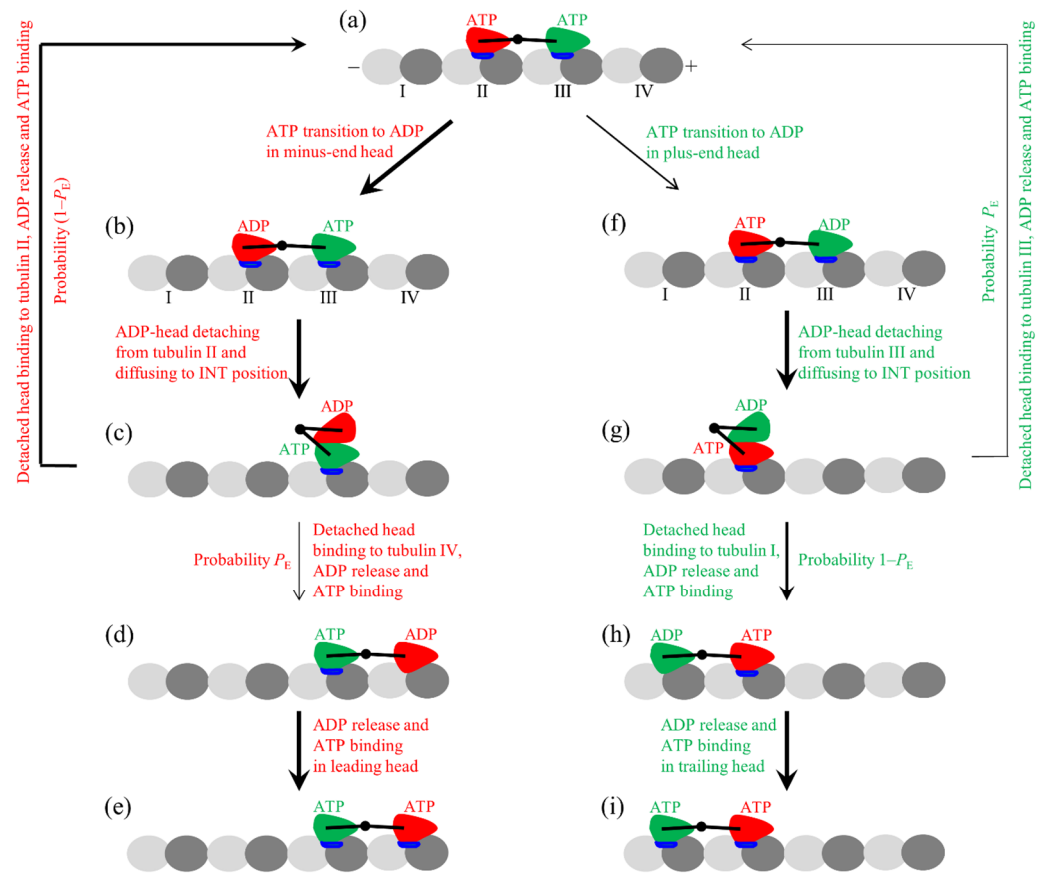


Figure 6. Schematic illustrations of the chemomechanical coupling for NcdKHC, the engineered motor consisting of the Ncd stalk and neck joined to the KHC motor domain. (a–i) The pathway at saturating ATP concentrations. At saturating ATP, the nucleotide-free state of the kinesin head is so short that is not needed to be considered. Since in both the ATP and ADP.Pi states the kinesin head has a similar conformation and has a high affinity to the MT, for simplicity, ATP hydrolysis and Pi release are treated as one step in the ATP transition to ADP. The thickness of an arrow indicates the relative magnitude of the probability of transition between two states connected by the arrow under no load.

As stated in Section 2.2, the rate of ATP transition to ADP of the minus-ended head is $k^{(+)}$ and that of the plus-ended head is $k^{(-)}$. Based on the pathway of Figure 6, Equations (1) and (2) for the ATPase rates of the minus- and plus-ended heads of the NcdKHC motor can be simplified as:

$$k_m = k^{(+)}P_E + \frac{k^{(+)}k_D}{k^{(+)} + k_D}(1 - P_E), \tag{8}$$

$$k_p = \frac{k^{(-)}k_D}{k^{(-)} + k_D}P_E + k^{(-)}(1 - P_E), \tag{9}$$

where the probability P_E still has the form of Equation (4). However, since under no load, the neck of the NcdKHC head in the ATP and ADP states tilts towards the minus- and plus-ended directions, respectively, E_{NL} should have a negative value. Equation (6) for the velocity of the NcdKHC motor can be simplified as:

$$v = [P_Ek_m - (1 - P_E)k_p]d. \tag{10}$$

Equation (7) for the number of ATP molecules consumed per forward step of the NcdKHC motor can be simplified as:

$$N = \frac{k_m + k_p}{P_E k_m}. \quad (11)$$

From Equations (8)–(11), it is seen that to calculate the velocity and number of ATPs per step, values of parameters k_D , $k^{(+)}$, $k^{(-)}$, E_0 , and δ are required. The kinesin-1 motor domain in the NcdKHC should have the same rate constants of the ATP activity and the same interaction potential with the MT as that in the WT kinesin-1. Thus, we have the same values of parameters k_D , $k^{(+)}$, $k^{(-)}$, and δ as those given in Table 2. Similarly, the free energy change E_C for the kinesin-1 motor domain in the NcdKHC should have the same value as that in the WT kinesin-1. However, the free energy change E_{NL} for the NcdKHC has a negative value. Here, we take $E_0 = E_C + E_{NL}$ for the NcdKHC to be variable. Under no load, the theoretical results of the velocity versus E_0 are shown in Figure 7a, with the enlargement of Figure 7a in the range of E_0 from $-2k_B T$ to $-1.4k_B T$ being shown in Figure 7b. From Figure 7a, it is seen that for the WT kinesin-1 with $E_0 = 4.5k_B T$, the velocity is $v = 44.56$ mm/min, which is close to the experimental value of 42.7 mm/min measured by Endow and Waligora for the KHC motor [40]. From Figure 7b, it is seen interestingly that at $E_0 = -1.91k_B T$, the theoretical velocity is consistent with the experimental value for the NcdKHC1 and NcdKHC6 [40], at $E_0 = -1.61k_B T$, the theoretical velocity is consistent with the experimental value for the NcdKHC2 and NcdKHC5 [40], and at $E_0 = -1.75k_B T$, the theoretical velocity is consistent with the experimental value for the NcdKHC4 [40], where the NcdKHC1-6 represent different mutations in the neck region [40]. Approximating that E_C and E_{NL} for the WT kinesin-1 have the same value (see above), giving $E_C = 2.25k_B T$, the above results imply $E_{NL} = -4.16k_B T$ for the NcdKHC1 and NcdKHC6, $E_{NL} = -3.86k_B T$ for the NcdKHC2 and NcdKHC5, and $E_{NL} = -4k_B T$ for the NcdKHC4. In other words, the total free energy of an Ncd head in the ATP state tilting towards the minus-ended orientation and an Ncd head in the ADP state tilting towards the plus-ended orientation has a small value of about $4k_B T$. This implies that the free energy of retaining the neck region of an Ncd head in the equilibrium orientation, which is about $2k_B T$, is similar to the NL-docking energy of a kinesin-1 head.

Furthermore, we provide predicted results on load dependences of the velocity and number of ATPs per step for the NcdKHC1 and NcdKHC6 and those for the NcdKHC2 and NcdKHC5, which are shown in Figure 7c,d, where for comparison the corresponding results for the WT kinesin-1 are also shown. From Figure 7c, it is seen interestingly that with the increase in the forward (plus-ended) load, the velocities of the NcdKHC1–6 increase significantly and become close to the WT case at the high forward load. With the increase in the magnitude of the backward (minus-ended) load, the velocities decrease and level out to a value with the magnitude of $k^{(-)}d$ being much smaller than the maximum velocity of $k^{(+)}d$ at the high forward load. From Figure 7d, it is seen interestingly that under no load, the numbers of ATPs per step are about 9.26 for the NcdKHC1 and NcdKHC6 and about 7.15 for the NcdKHC2 and NcdKHC5, which is in contrast to the WT case with the number of ATPs per step being close to 1. With the increase in the magnitude of the backward load, the numbers of ATPs per step for the NcdKHC1–6 increase significantly. With the increase in the magnitude of the forward load, the numbers of ATPs per step for the NcdKHC1–6 decrease and become close to the WT case at the high forward load. These predicted results shown in Figure 7c,d can be tested using future single-molecule optical trapping experiments.

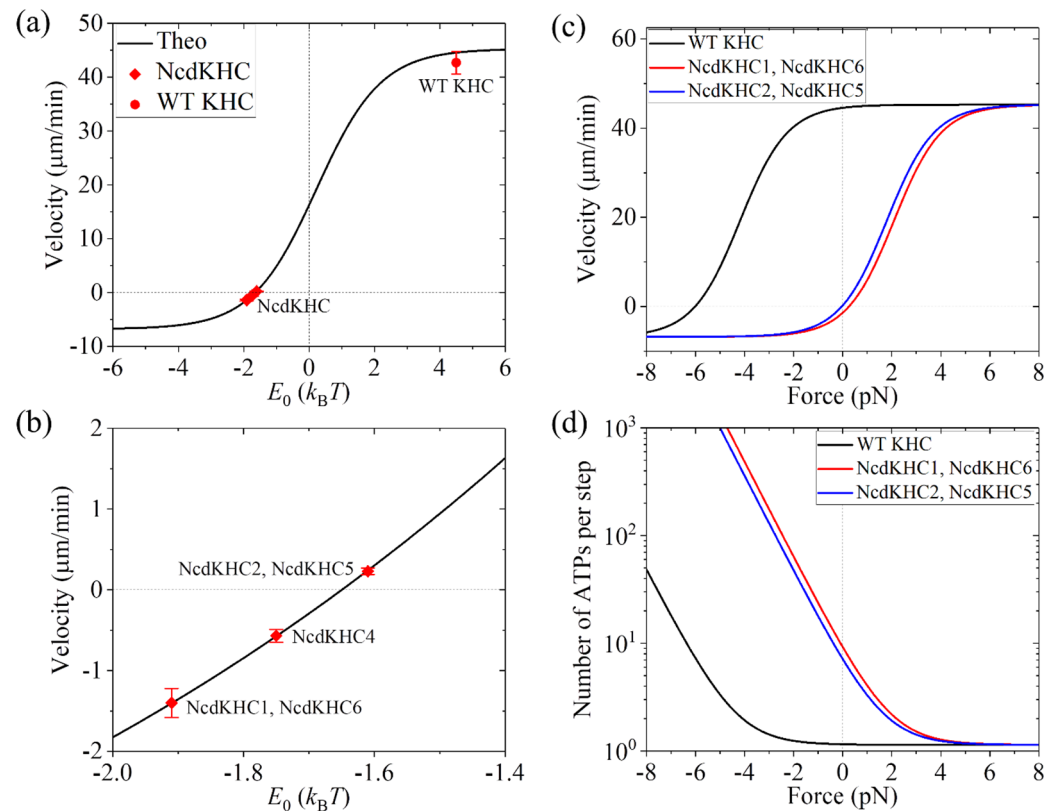


Figure 7. Dynamics of NcdKHC motors. WT and NcdHKCs represent the wild-type K560 and the engineered motor consisting of the Ncd stalk and neck joined to the KHC motor domain, respectively. Lines are theoretical results. Symbols are experimental data taken from Endow and Waligora [40]. (a) Velocity versus E_0 under no load. (b) Enlargement of (a) in the range of E_0 from $-2k_B T$ to $-1.4k_B T$. (c) Velocity versus backward and forward loads for the WT and NcdHKCs. (d) Number of ATPs consumer per step versus backward and forward loads for the WT and NcdHKCs.

3.6. Dynamics of Motor with Kinesin-1 Neck and NL Joined to the Ncd Motor Domain

In this section, we consider the engineered motor with the human kinesin-1 catalytic domain (316 residues) in a dimeric construct (560 residues) being replaced with the catalytic domain of Ncd, as performed in the experiments of Case et al. [41]. The engineered motor is called KHCNcd here. The pathway for the KHCNcd can still be described schematically as that shown in Figure 1.

For the Ncd motor domain in the KHCNcd dimer, it is reasonably considered that the orientation of kinesin-1 NL has no effect on the rate of ATP transition to ADP. Thus, both the minus- and plus-ended heads of the KHCNcd dimer have the same rates of ATP transition to ADP, which are denoted by $k^{(+)}$ and $k^{(-)}$ (with $k^{(+)} = k^{(-)}$), respectively, and $E_C = 0$. When the kinesin-1 NL is in the plus-ended orientation (e.g., for the NL of the minus-ended head in Figure 1a), it has a large contacting area with the Ncd motor domain, and thus some residues in the NL can form interactions with residues in the motor domain, giving a small binding energy (still denoted by E_{NL}), which should be evidently smaller than the NL-docking energy for the WT kinesin-1. By contrast, when the kinesin-1 NL is the minus-ended orientation (e.g., for the NL of the plus-ended head in Figure 1a), it has a little contacting area with the Ncd motor domain and thus nearly no residue in the NL can interact with that in the motor domain. This implies that the minus-ended head has a small ‘NL-docking’ energy of E_{NL} while the plus-ended head has no ‘NL-docking’ energy, giving $E_0 = E_{NL}$ because $E_C = 0$ (see just above). Since the kinesin-1 NL has a short length, we take $P_0 = 1$. Thus, during the processive stepping of the KHCNcd motor, the overall ATPase rates of the heads in the minus- and plus-ended positions still have forms of Equations (8) and (9), respectively, but with $k^{(+)} = k^{(-)}$. The velocity and number of ATPs per step of the

KHCNcd can still be calculated with Equations (10) and (11), respectively. The probability P_E still has the form of Equation (4). Considering one step per ATP for the WT Ncd motor, from the measured velocity of 140 nm/s [41] we have $k^{(+)} = k^{(-)} = 17.1 \text{ s}^{-1}$. We still take $k_D = 250 \text{ s}^{-1}$. Then, using Equations (8)–(11), the calculated results of velocity versus E_0 are shown in Figure 8a. As expected, at $E_0 = 0$, the velocity is zero. With the increase in E_0 , the velocity increases and levels out to the value of $k^{(+)}d$ at high E_0 . Interestingly, it is noted that at $E_0 = 0.92k_B T$, the theoretical velocity is consistent with the experimental value for the KHCNcd dimer measured by Case et al. [41]. This implies that $E_{NL} = 0.92k_B T$. As expected, this value of E_{NL} is evidently smaller than the NL-docking energy for the WT kinesin-1 (see just above).

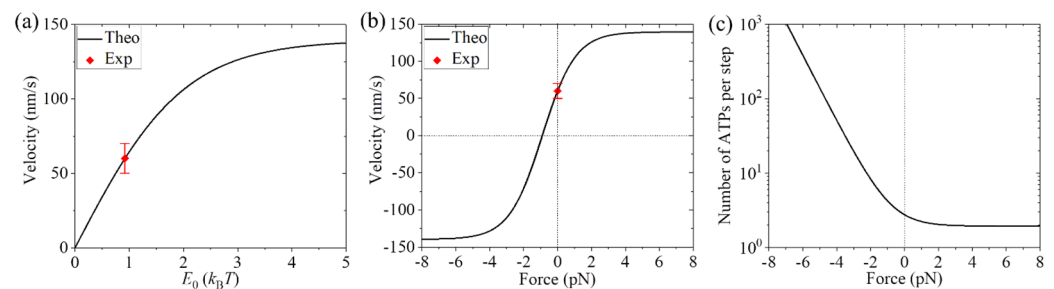


Figure 8. Dynamics of KHCNcd motors. KHCNcd represents the engineered motor consisting of the neck and NL of kinesin-1 joined to the Ncd motor domain. Lines are theoretical results. Symbols are experimental data taken from Case et al. [41]. (a) Velocity versus E_0 under no load. (b) Velocity versus backward and forward loads. (c) Number of ATPs consumer per step versus backward and forward loads.

Furthermore, we provide predicted results on load dependences of the velocity and number of ATPs per step for the KHCNcd, which are shown in Figure 8b,c. From Figure 8b, it is seen interestingly that with the increase in the forward (plus-ended) load, the velocity of the KHCNcd increases and levels out to the value of $k^{(+)}d$ at the high forward load. With the increase in the magnitude of the backward (minus-ended) load, the velocity decreases and becomes negative at the load of about -0.9 pN , implying that the stall force is about 0.9 pN . At the high backward load, the velocity levels out to the value with the magnitude of $k^{(-)}d$ equal to the corresponding one of $k^{(+)}d$ at the high forward load. From Figure 8c, it is seen interestingly that under no load, the number of ATPs per step is about 3. With the increase in the magnitude of the backward load, the number of ATPs per step increases significantly. With the increase in the forward load, the number of ATPs per step decreases and becomes close to 1 at the high forward load. These predicted results shown in Figure 8b,c can be tested using future single-molecule optical trapping experiments.

4. Discussion

In the Results section, we focused mainly on the effects of NL docking on the motility of kinesin-1, kinesin-2, NcdKHC, and KHCNcd motors. Here, we discuss the effects of NL docking on the motility of other families of kinesin motors such as kinesin-6 MKLP2 and kinesin-5 Cin8.

4.1. Unidirectional Motility of Kinesin-6 MKLP2

The mitotic kinesin-like protein 2, MKLP2, is a member of the kinesin-6 family, playing critical roles during the metaphase–anaphase transition and cytokinesis [71–75]. The available structural data for MKLP2 indicated that although there exists a large conformational change of the head in the ATP state compared to that in the ϕ state, no NL docking occurs in the ATP-head [76]. However, the available experimental data showed that the MKLP2 dimer can also move processively towards the plus end [77], such as the kinesin-1 and kinesin-2 dimers. Based on the studies here, for the MKLP2 dimer, we have $E_{NL} = 0$, giving $E_0 = E_C$, and thus the processive movement of the MKLP2 dimer can be readily

explained, similar to the case for the kinesin-1 dimer with the deletion of the cover strand (see Section 3.1) and that for the kinesin-2 dimer with its NL being swapped with that of kinesin-1 (see Section 3.4).

4.2. Effect of NL Mutation on Motility of bi-Directional Kinesin-5 Cin8

While most members of the kinesin-5 family such as vertebrate Eg5 and *Drosophila* Klp61F can move processively towards the plus end [78,79], such as the kinesin-1 and kinesin-2 motors, three fungal kinesin-5 motors—*S. cerevisiae* Cin8 and Kip1 and *S. pombe* Cut7—can move processively towards either the plus or minus end, which depends on the experimental conditions [80–85], although their NLs can always be docked in the plus-ended direction [84,85]. For example, under the high or physiological ionic strength condition, the single Cin8, Kip1, and Cut7 motors can move processively towards the minus end, whereas under the low ionic strength condition, they can transit to move processively towards the plus end [80–85].

Recently, the effect of the NL mutation on the motility of the bi-directional Cin8 was studied by Goldstein-Levitin et al. [86]. It was found that under the high ionic strength condition, the NL variants of Cin8 motors with the destabilization of the NL docking can still move directionally towards the minus end, such as the WT Cin8 motor [86]. By contrast, the NL variant with the additional stabilization of the NL docking, which was generated by the replacement of the NL of Cin8 with sequences of Eg5, exhibited only bi-directional motility, with no minus-end directed bias, in contrast to the WT Cin8 motor [86]. For convenience, the variant of Cin8 with the destabilization of the NL docking is called Cin8_{NL}MT here, while that with the additional stabilization of the NL docking is called Cin8_{NL}Eg5. Moreover, Goldstein-Levitin et al. [86] found that the Cin8_{NL}MT motors exhibit an impaired ability and Cin8_{NL}Eg5 motors exhibit a more impaired ability to crosslink and/or slide apart two antiparallel MTs in vitro and in vivo, in contrast to the WT Cin8 motors. Here, we provide an explanation of the above experimental results for the WT Cin8 and its variants.

As proposed before, both the bidirectional Cin8 and the unidirectional kinesin-1 motors show a similar chemomechanical coupling mechanism [87]. Thus, the pathway for the Cin8 can also be shown in Figure 1 [87]. The only differences between the Cin8 and kinesin-1 motors were proposed as follows [87]. (i) For Cin8, the minus-ended ATP-head with the closed NBP and the large conformational change has a different strong affinity to the MT from the plus-ended head with the open NBS and without the large conformational change, with the former equivalent to the head in the ATP state and the latter equivalent to the head in the ϕ state. Thus, it was proposed that the large conformational modulations of the local tubulin induced by the strong interaction with the minus-ended ATP-head are different from those induced by the strong interaction with the plus-ended ATP-head, resulting in $P_0^{(0)}$ for the plus-ended ADP-head being smaller than that for the minus-ended ADP-head [87] (for convenience, with $P_0^{(0)}$ for the minus- and plus-ended heads being denoted by $P_0^{(0T)}$ and $P_0^{(0L)}$, respectively). For kinesin-1, for simplicity, we take the minus- and plus-ended ADP-heads as having the same value of $P_0^{(0)}$ in the Results section. (ii) In contrast to the proposal for kinesin-1 that the minus-ended head has a larger rate of ATP transition to ADP than the plus-ended head, for the Cin8, it was proposed that the minus-ended head has a smaller rate of ATP transition to ADP than the plus-ended head [87]. From Equation (6), the velocity of the Cin8 under no load has the form:

$$v = \left[P_0^{(0T)} P_E k_T - P_0^{(0L)} (1 - P_E) k_L \right] d, \quad (12)$$

where P_E still has the form of Equation (4). Under no load, Equation (4) can be simplified as:

$$P_E = \frac{\exp(\beta E_0)}{\exp(\beta E_0) + 1}. \quad (13)$$

From Equations (1) and (2), considering $k_D \gg k^{(+)}$ and $k_D \gg k^{(-)}$, we approximately have $k_T = k^{(+)}$ and $k_L = k^{(-)}$. Thus, Equation (12) can be approximately rewritten as:

$$v = \frac{1}{\exp(\beta E_0) + 1} \left[P_0^{(OT)} \exp(\beta E_0) k^{(+)} - P_0^{(OL)} k^{(-)} \right] d. \quad (14)$$

First, consider the single WT Cin8 motor. Under the high ionic strength condition, we take $P_0^{(OL)} \approx 1$ and $P_0^{(OT)} \approx 1$, as for the WT kinesin-1. Since the Cin8 has a smaller NL-docking energy than the kinesin-1, implying that the Cin8 has a small value of E_0 , from Equation (14), we thus note that if $\exp(\beta E_0) < k^{(-)}/k^{(+)}$, we have a negative value of v , implying the minus-end directed movement. Under the low ionic strength condition, the affinity of the head to the MT will be increased. Thus, $P_0^{(OL)}$ and $P_0^{(OT)}$ can become smaller than 1, but with $P_0^{(OL)} < P_0^{(OT)}$ (see above). Thus, from Equation (14), we note that if $\exp(\beta E_0) P_0^{(OT)}/P_0^{(OL)} > k^{(-)}/k^{(+)}$, we have a positive value of v , implying the plus-end directed movement. In other words, if $\exp(\beta E_0) < k^{(-)}/k^{(+)} < \exp(\beta E_0) P_0^{(OT)}/P_0^{(OL)}$, the Cin8 can move towards the minus end under the high ionic strength condition, whereas it can move towards the plus end under the low ionic strength condition, explaining the experimental data [81,84,86]. For example, by taking $E_0 = 0.8k_B T$, $k^{(+)} = 15 \text{ s}^{-1}$, and $k^{(-)} = 158 \text{ s}^{-1}$, we have $v \approx -320 \text{ nm/s}$ under the high ionic strength condition (with $P_0^{(OL)} \approx P_0^{(OT)} \approx 1$) and $v \approx 80 \text{ nm/s}$ under the low ionic strength condition (with $P_0^{(OL)} \approx 0.01$ and $P_0^{(OT)} \approx 1$), which are close to the experimental data [81,86].

Then, consider the single Cin8_{NL}MT and Cin8_{NL}Eg5 motors. As mentioned above, E_0 for the Cin8_{NL}MT is smaller than that for the WT Cin8. Thus, it is still expected that $\exp(\beta E_0) < k^{(-)}/k^{(+)}$ for the Cin8_{NL}MT motor. Consequently, from Equation (14), and considering $P_0^{(OL)} \approx 1$ and $P_0^{(OT)} \approx 1$ under the high ionic strength condition (see above), the Cin8_{NL}MT motor can move towards the minus end, similar to the WT Cin8 motor, explaining the experimental data [86]. The observed velocity of the Cin8_{NL}MT motor, which is smaller than that of the WT Cin8 motor [86], could be due to the mutations increasing the ATPase rate of the minus-ended head, $k^{(+)}$, and/or decreasing the ATPase rate of the plus-ended head, $k^{(-)}$. As mentioned above, E_0 for the Cin8_{NL}Eg5 motor is larger than that for the WT Cin8 motor. Thus, compared to the case for the WT Cin8 motor, the Cin8_{NL}Eg5 motor $\exp(\beta E_0)$ can increase to a value nearly equal to that of $k^{(-)}/k^{(+)}$. Consequently, from Equation (14), and considering $P_0^{(OL)} \approx 1$ and $P_0^{(OT)} \approx 1$ under the high ionic strength condition (see above), we see that the Cin8_{NL}Eg5 moves bi-directionally, with neither minus-end nor plus-end directed bias, explaining the experimental data [86].

As explained before [87], under the high ionic strength condition, the sliding of the two antiparallel MTs by multiple Cin8 motors that move in the plus-ended direction is due to the MT-bound Cin8 bound by other detached Cin8, and thus the reduction of $P_0^{(OL)}$ for the MT-bound Cin8. As previous studies on the Eg5 motors showed, the reason that the full-length Eg5 motors can slide apart two antiparallel MTs, whereas the Eg5 motors with deletion of their tail domains cannot, arises mainly from the former motors having a smaller dissociation rate than the latter motors [88]. Thus, the impaired ability of the Cin8_{NL}MT motors to crosslink and slide apart two antiparallel MTs is also mainly due to the large dissociation rate that results from the low affinity to the MT, as shown in Goldstein-Levitin et al. [86]. The more impaired ability of the Cin8_{NL}Eg5 motors to crosslink and/or slide apart two antiparallel MTs is due to both the low affinity to MTs [86] and the low probability of the MT-bound Cin8_{NL}Eg5 bound by other detached Cin8_{NL}Eg5, which results from the abolished ability to localize near the minus ends by the minus-end directed motility.

5. Conclusions

The effects of the NL on the dynamics of kinesin dimers are studied analytically based on our proposed model, explaining quantitatively diverse experimental data on the mutations related to the NL docking and moreover providing predicted results. For example, the puzzling experimental results showing that the kinesin-1 with the deletion of the cover strand contributing to the NL docking, implying the nullification of the NL docking, can still move processively towards the plus end with the velocity similar to the WT case are explained quantitatively. The puzzling experimental data showing that the kinesin-2 dimer with the NL being swapped with that of kinesin-1, implying no occurrence of the NL docking, behaves similar to the WT kinesin-2 dimer are explained well. The experimental data about the effect of the extension of the NL of kinesin-1, the effect of the mutation of the NL region and residues that can interact with the NL region in the motor domain of kinesin-1, the effect of joining the stalk and neck of Ncd to the motor domain of kinesin-1, the effect of the replacement of the motor domain of kinesin-1 with that of Ncd, etc., on the motility of the motor are explained quantitatively. Similarly, the processive motility of kinesin-6 MKLP2 with no NL docking can also be explained readily. Additionally, the available experimental data about the effects of NL mutations on the dynamics of the bi-directional kinesin-5 Cin8 can also be explained well. In conclusion, the studies in this work indicate clearly that the NL docking does not play a critical role and only plays an assistant role in the motility of the kinesin dimer.

Finally, it is mentioned that the theoretical study of the dynamics of the kinesin motors related to the NL here is on the basis of the kinetic model. A future study is hoped to directly test the argument that the mutations of the NL region and residues that can interact with the NL region in the kinesin-1's motor domain can affect its conformation (see Section 3.3) by using the detailed molecular dynamics simulations such as with the structure-based coarse-grained modeling [68,69].

Funding: This research received no external funding.

Institutional Review Board Statement: Not applicable.

Informed Consent Statement: Not applicable.

Data Availability Statement: All data are included in the text.

Conflicts of Interest: The author declares no conflict of interest.

References

1. Vale, R.D.; Reese, T.S.; Sheetz, M.P. Identification of a novel force-generating protein, kinesin, involved in microtubule-based motility. *Cell* **1985**, *42*, 39–50. [[CrossRef](#)]
2. Kozielski, F.; Sack, S.; Marx, A.; Thormahlen, M.; Schonbrunn, E.; Biou, V.; Thompson, A.; Mandelkow, E.-M.; Mandelkow, E. The crystal structure of dimeric kinesin and implications for microtubule-dependent motility. *Cell* **1997**, *91*, 985–994. [[CrossRef](#)]
3. Lawrence, C.J.; Dawe, R.K.; Christie, K.R.; Cleveland, D.W.; Dawson, S.C.; Endow, S.A.; Wordeman, L. A standardized kinesin nomenclature. *J. Cell Biol.* **2004**, *167*, 19–22. [[CrossRef](#)] [[PubMed](#)]
4. Howard, J. The movement of kinesin along microtubules. *Annu. Rev. Physiol.* **1996**, *58*, 703–729. [[CrossRef](#)] [[PubMed](#)]
5. Cross, R.A. The kinetic mechanism of kinesin. *Trends Biochem. Sci.* **2004**, *29*, 301–309. [[CrossRef](#)] [[PubMed](#)]
6. Asbury, C.L. Kinesin: World's tiniest biped. *Curr. Opin. Cell Biol.* **2005**, *17*, 89–97. [[CrossRef](#)]
7. Block, S.M. Kinesin motor mechanics: Binding, stepping, tracking, gating, and limping. *Biophys. J.* **2007**, *92*, 2986–2995. [[CrossRef](#)] [[PubMed](#)]
8. Xie, P. Insight into the chemomechanical coupling mechanism of kinesin molecular motors. *Commun. Theor. Phys.* **2021**, *73*, 057601. [[CrossRef](#)]
9. Gigant, B.; Wang, W.; Dreier, B.; Jiang, Q.; Pecqueur, L.; Plückthun, A.; Wang, C.; Knossow, M. Structure of a kinesin-tubulin complex and implications for kinesin motility. *Nat. Struct. Mol. Biol.* **2013**, *20*, 1001–1007. [[CrossRef](#)]
10. Cao, L.; Wang, W.; Jiang, Q.; Wang, C.; Knossow, M.; Gigant, B. The structure of apo-kinesin bound to tubulin links the nucleotide cycle to movement. *Nat. Commun.* **2014**, *5*, 5364. [[CrossRef](#)]
11. Cross, R.A. Mechanochemistry of the kinesin-1 ATPase. *Biopolymers* **2016**, *105*, 476–482. [[CrossRef](#)] [[PubMed](#)]
12. Visscher, K.; Schnitzer, M.J.; Block, S.M. Single Kinesin Molecules Studied with a Molecular Force Clamp. *Nature* **1999**, *400*, 184–189. [[CrossRef](#)] [[PubMed](#)]

13. Coppin, C.M.; Pierce, D.W.; Hsu, L.; Vale, R.D. The load dependence of kinesin's mechanical cycle. *Proc. Natl. Acad. Sci. USA* **1997**, *94*, 8539–8544. [[CrossRef](#)] [[PubMed](#)]
14. Nishiyama, M.; Higuchi, H.; Yanagida, T. Chemomechanical Coupling of the Forward and Backward Steps of Single Kinesin Molecules. *Nat. Cell Biol.* **2002**, *4*, 790–797. [[CrossRef](#)]
15. Carter, N.J.; Cross, R.A. Mechanics of the Kinesin Step. *Nature* **2005**, *435*, 308–312. [[CrossRef](#)]
16. Taniguchi, Y.; Nishiyama, M.; Ishii, Y.; Yanagida, T. Entropy rectifies the Brownian steps of kinesin. *Nat. Chem. Biol.* **2005**, *1*, 342–347. [[CrossRef](#)] [[PubMed](#)]
17. Fisher, M.E.; Kolomeisky, A.B. Simple mechanochemistry describes the dynamics of kinesin molecules. *Proc. Natl. Acad. Sci. USA* **2001**, *98*, 7748–7753. [[CrossRef](#)]
18. Liepelt, S.; Lipowsky, R. Kinesin's network of chemomechanical motor cycles. *Phys. Rev. Lett.* **2007**, *98*, 258102. [[CrossRef](#)]
19. Hyeon, C.; Onuchic, J.N. Internal strain regulates the nucleotide binding site of the kinesin leading head. *Proc. Natl. Acad. Sci. USA* **2007**, *104*, 2175–2180. [[CrossRef](#)] [[PubMed](#)]
20. Sumi, T. Design principles governing chemomechanical coupling of kinesin. *Sci. Rep.* **2017**, *7*, 1163. [[CrossRef](#)] [[PubMed](#)]
21. Hyeon, C.; Klumpp, S.; Onuchic, J.N. Kinesin's backsteps under mechanical load. *Phys. Chem. Chem. Phys.* **2009**, *11*, 4899–4910. [[CrossRef](#)] [[PubMed](#)]
22. Sasaki, K.; Kaya, M.; Higuchi, H. A unified walking model for dimeric motor proteins. *Biophys. J.* **2018**, *115*, 1–12. [[CrossRef](#)] [[PubMed](#)]
23. Xie, P.; Guo, S.-K.; Chen, H. ATP-concentration- and force-dependent chemomechanical coupling of kinesin molecular motors. *J. Chem. Inf. Model.* **2019**, *59*, 360–372. [[CrossRef](#)] [[PubMed](#)]
24. Mugnai, M.L.; Hyeon, C.; Hinczewski, M.; Thirumalai, D. Theoretical perspectives on biological machines. *Rev. Mod. Phys.* **2020**, *92*, 025001. [[CrossRef](#)]
25. Vale, R.D.; Milligan, R.A. The way things move: Looking under the hood of molecular motor proteins. *Science* **2000**, *288*, 88–95. [[CrossRef](#)] [[PubMed](#)]
26. Endow, S.A.; Barker, D.S. Processive and nonprocessive models of kinesin movement. *Annu. Rev. Physiol.* **2003**, *65*, 161–175. [[CrossRef](#)]
27. Klumpp, L.M.; Hoenger, A.; Gilbert, S.P. Kinesin's second step. *Proc. Natl. Acad. Sci. USA* **2004**, *101*, 3444–3449. [[CrossRef](#)] [[PubMed](#)]
28. Rosenfeld, S.S.; Fordyce, P.M.; Jefferson, G.M.; King, P.H.; Block, S.M. Stepping and stretching: How kinesin uses internal strain to walk processively. *J. Biol. Chem.* **2003**, *278*, 18550–18556. [[CrossRef](#)]
29. Schief, W.R.; Howard, J. Conformational changes during kinesin motility. *Curr. Opin. Cell Biol.* **2001**, *13*, 19–28. [[CrossRef](#)]
30. Mori, T.; Vale, R.D.; Tomishige, M. How kinesin waits between steps. *Nature* **2007**, *450*, 750–754. [[CrossRef](#)]
31. Sack, S.; Muller, J.; Marx, A.; Thormahlen, M.; Mandelkow, E.-M.; Brady, S.T.; Mandelkow, E. X-ray structure of motor and neck domains from rat brain kinesin. *Biochemistry* **1997**, *36*, 16155–16165. [[CrossRef](#)] [[PubMed](#)]
32. Sindelar, C.V.; Budny, M.J.; Rice, S.; Naber, N.; Fletterick, R.; Cooke, R. Two conformations in the human kinesin power stroke defined by X-ray crystallography and EPR spectroscopy. *Nat. Struct. Biol.* **2002**, *9*, 844–848. [[CrossRef](#)] [[PubMed](#)]
33. Hwang, W.; Lang, M.J.; Karplus, M. Force generation in kinesin hinges on cover-neck bundle formation. *Structure* **2008**, *16*, 62–71. [[CrossRef](#)] [[PubMed](#)]
34. Khalil, A.S.; Appleyard, D.C.; Labno, A.K.; Georges, A.; Karplus, M.; Belcher, A.M.; Hwang, W.; Lang, M.J. Kinesin's cover-neck bundle folds forward to generate force. *Proc. Natl. Acad. Sci. USA* **2008**, *105*, 19247–19252. [[CrossRef](#)] [[PubMed](#)]
35. Budaitis, B.G.; Jariwala, S.; Reinemann, D.N.; Schimert, K.I.; Scarabelli, G.; Grant, B.J.; Sept, D.; Lang, M.J.; Verhey, K.J. Neck linker docking is critical for Kinesin-1 force generation in cells but at a cost to motor speed and processivity. *eLife* **2019**, *8*, e44146. [[CrossRef](#)] [[PubMed](#)]
36. Clancy, B.E.; Behnke-Parks, W.M.; Andreasson, J.O.L.; Rosenfeld, S.S.; Block, S.M. A universal pathway for kinesin stepping. *Nat. Struct. Mol. Biol.* **2011**, *18*, 1020–1027. [[CrossRef](#)]
37. Andreasson, J.O.L.; Milic, B.; Chen, G.-Y.; Guydosh, N.R.; Hancock, W.O.; Block, S.M. Examining kinesin processivity within a general gating framework. *eLife* **2015**, *4*, e07403. [[CrossRef](#)]
38. Case, R.B.; Rice, S.; Hart, C.L.; Ly, B.; Vale, R.D. Role of the kinesin neck linker and catalytic core in microtubule-based motility. *Curr. Biol.* **2000**, *10*, 157–160. [[CrossRef](#)]
39. Andreasson, J.O.L.; Shastry, S.; Hancock, W.O.; Block, S.M. The mechanochemical cycle of mammalian kinesin-2 KIF3A/B under load. *Curr. Biol.* **2015**, *25*, 1166–1175. [[CrossRef](#)]
40. Endow, S.A.; Waligora, K.W. Determinants of kinesin motor polarity. *Science* **1998**, *281*, 1200–1202. [[CrossRef](#)]
41. Case, R.B.; Pierce, D.W.; Hom-Booher, N.; Hart, C.L.; Vale, R.D. The directional preference of kinesin motors is specified by an element outside of the motor catalytic domain. *Cell* **1997**, *90*, 959–966. [[CrossRef](#)] [[PubMed](#)]
42. Henningsen, U.; Schliwa, M. Reversal in the direction of movement of a molecular motor. *Nature* **1997**, *389*, 93–96. [[CrossRef](#)]
43. Xie, P.; Guo, S.-K.; Chen, H. A generalized kinetic model for coupling between stepping and ATP hydrolysis of kinesin molecular motors. *Int. J. Mol. Sci.* **2019**, *20*, 4911. [[CrossRef](#)] [[PubMed](#)]
44. Xie, P. Dynamics of kinesin motor proteins under longitudinal and sideways loads. *J. Theor. Biol.* **2021**, *530*, 110879. [[CrossRef](#)]
45. Crevel, I.M.T.C.; Lockhart, A.; Cross, R.A. Weak and strong states of kinesin and Ncd. *J. Mol. Biol.* **1996**, *257*, 66–76. [[CrossRef](#)] [[PubMed](#)]

46. Sosa, H.; Peterman, E.J.G.; Moerner, W.E.; Goldstein, L.S.B. ADP-induced rocking of the kinesin motor domain revealed by single-molecule fluorescence polarization microscopy. *Nat. Struct. Biol.* **2001**, *8*, 540–544. [[CrossRef](#)] [[PubMed](#)]
47. Morikawa, M.; Yajima, H.; Nitta, R.; Inoue, S.; Ogura, T.; Sato, C.; Hirokawa, N. X-ray and Cryo-EM structures reveal mutual conformational changes of kinesin and GTP-state microtubules upon binding. *EMBO J.* **2015**, *34*, 1270–1286. [[CrossRef](#)]
48. Shi, X.-X.; Fu, Y.B.; Guo, S.K.; Wang, P.Y.; Chen, H.; Xie, P. Investigating role of conformational changes of microtubule in regulating its binding affinity to kinesin by all-atom molecular dynamics simulation. *Proteins* **2018**, *86*, 1127–1139. [[CrossRef](#)]
49. Shi, X.-X.; Wang, P.-Y.; Chen, H.; Xie, P. Studies of conformational changes of tubulin induced by interaction with kinesin using atomistic molecular dynamics simulations. *Int. J. Mol. Sci.* **2021**, *22*, 6709. [[CrossRef](#)]
50. Xie, P. Modeling processive motion of kinesin-13 MCAK and kinesin-14 Cik1-Kar3 molecular motors. *Protein Sci.* **2021**, *30*, 2092–2105. [[CrossRef](#)]
51. Shang, Z.; Zhou, K.; Xu, C.; Csencsits, R.; Cochran, J.C.; Sindelar, C.V. High-resolution structures of kinesin on microtubules provide a basis for nucleotide-gated force-generation. *eLife* **2014**, *3*, e04686. [[CrossRef](#)] [[PubMed](#)]
52. Kikkawa, M.; Hirokawa, N. High-resolution cryo-EM maps show the nucleotide binding pocket of KIF1A in open and closed conformations. *EMBO J.* **2006**, *25*, 4187–4194. [[CrossRef](#)] [[PubMed](#)]
53. Benoit, M.P.M.H.; Asenjo, A.B.; Paydar, M.; Dhakal, S.; Kwok, B.H.; Sosa, H. Structural basis of mechano-chemical coupling by the mitotic kinesin KIF14. *Nat. Commun.* **2021**, *12*, 3637. [[CrossRef](#)] [[PubMed](#)]
54. Rice, S.; Lin, A.W.; Safer, D.; Hart, C.L.; Naber, N.; Carragher, B.O.; Cain, S.M.; Pechatnikova, E.; Wilson-Kubalek, E.M.; Whittaker, M.; et al. A structural change in the kinesin motor protein that drives motility. *Nature* **1999**, *402*, 778–784. [[CrossRef](#)] [[PubMed](#)]
55. Tomishige, M.; Vale, R.D. Controlling kinesin by reversible disulfide crosslinking. Identifying the motility-producing conformational change. *J. Cell Biol.* **2000**, *151*, 1081–1092. [[CrossRef](#)]
56. Asenjo, A.B.; Weinberg, Y.; Sosa, H. Nucleotide binding and hydrolysis induces a disorder-order transition in the kinesin neck-linker region. *Nat. Struct. Mol. Biol.* **2006**, *13*, 648–654. [[CrossRef](#)] [[PubMed](#)]
57. Shi, X.-X.; Guo, S.-K.; Wang, P.-Y.; Chen, H.; Xie, P. All-atom molecular dynamics simulations reveal how kinesin transits from one-head-bound to two-heads-bound state. *Proteins* **2020**, *88*, 545–557. [[CrossRef](#)]
58. Nitta, R.; Okada, Y.; Hirokawa, N. Structural model for strain-dependent microtubule activation of Mg-ADP release from kinesin. *Nat. Struct. Mol. Biol.* **2008**, *15*, 1067–1075. [[CrossRef](#)]
59. Moyer, M.L.; Gilbert, S.P.; Johnson, K.A. Pathway of ATP hydrolysis by monomeric and dimeric kinesin. *Biochemistry* **1998**, *37*, 800–813. [[CrossRef](#)]
60. Okada, Y.; Hirokawa, N. A processive single-headed motor: Kinesin superfamily protein KIF1A. *Science* **1999**, *283*, 1152–1157. [[CrossRef](#)]
61. Yildiz, A.; Tomishige, M.; Gennerich, A.; Vale, R.D. Intramolecular strain coordinates kinesin stepping behavior along microtubules. *Cell* **2008**, *134*, 1030–1041. [[CrossRef](#)] [[PubMed](#)]
62. Rosenfeld, S.S.; Jefferson, G.M.; King, P.H. ATP reorients the neck linker of kinesin in two sequential steps. *J. Biol. Chem.* **2001**, *276*, 40167–40174. [[CrossRef](#)]
63. Xie, P. Molecular mechanism of processive stepping of kinesin motors. *Symmetry* **2021**, *13*, 1799. [[CrossRef](#)]
64. Guo, S.-K.; Wang, P.-Y.; Xie, P. A model of processive movement of dimeric kinesin. *J. Theor. Biol.* **2017**, *414*, 62–75. [[CrossRef](#)]
65. Rice, S.; Cui, Y.; Sindelar, C.; Naber, N.; Matuska, M.; Vale, R.; Cooke, R. Thermodynamic properties of the kinesin neck region docking to the catalytic core. *Biophys. J.* **2003**, *84*, 1844–1854. [[CrossRef](#)] [[PubMed](#)]
66. Hwang, W.; Lang, M.J.; Karplus, M. Kinesin motility is driven by subdomain dynamics. *eLife* **2017**, *6*, e28948. [[CrossRef](#)]
67. Xie, P. Non-tight and tight chemomechanical couplings of biomolecular motors under hindering loads. *J. Theor. Biol.* **2020**, *490*, 110173. [[CrossRef](#)]
68. Togashi, Y.; Flechsig, H. Coarse-Grained Protein Dynamics Studies Using Elastic Network Models. *Int. J. Mol. Sci.* **2018**, *19*, 3899. [[CrossRef](#)] [[PubMed](#)]
69. Loutchko, D.; Flechsig, H. Allosteric communication in molecular machines via information exchange: What can be learned from dynamical modeling. *Biophys. Rev.* **2020**, *12*, 443–452. [[CrossRef](#)]
70. Endres, N.F.; Yoshioka, C.; Milligan, R.A.; Vale, R.D. A lever-arm rotation drives motility of the minus-end-directed kinesin Ncd. *Nature* **2006**, *439*, 875–878. [[CrossRef](#)]
71. Gruneberg, U.; Neef, R.; Honda, R.; Nigg, E.A.; Barr, F.A. Relocation of aurora B from centromeres to the central spindle at the metaphase to anaphase transition requires MKlp2. *J. Cell Biol.* **2004**, *166*, 167–172. [[CrossRef](#)] [[PubMed](#)]
72. Cesario, J.M.; Jang, J.K.; Redding, B.; Shah, N.; Rahman, T.; McKim, K.S. Kinesin 6 family member Subito participates in mitotic spindle assembly and interacts with mitotic regulators. *J. Cell Sci.* **2006**, *119*, 4770–4780. [[CrossRef](#)] [[PubMed](#)]
73. Hummer, S.; Mayer, T.U. Cdk1 negatively regulates midzone localization of the mitotic kinesin Mklp2 and the chromosomal passenger complex. *Curr. Biol.* **2009**, *19*, 607–612. [[CrossRef](#)] [[PubMed](#)]
74. Kitagawa, M.; Fung, S.Y.S.; Onishi, N.; Saya, H.; Lee, S.H. Targeting aurora B to the equatorial cortex by MKlp2 is required for cytokinesis. *PLoS ONE* **2013**, *8*, e64826. [[CrossRef](#)] [[PubMed](#)]
75. Landino, J.; Norris, S.R.; Li, M.; Ballister, E.R.; Lampson, M.A.; Ohi, R. Two mechanisms coordinate the recruitment of the chromosomal passenger complex to the plane of cell division. *Mol. Biol. Cell* **2017**, *28*, 3634–3646. [[CrossRef](#)]
76. Atherton, J.; Yu, I.-M.; Cook, A.; Muretta, J.M.; Joseph, A.; Major, J.; Sourigues, Y.; Clause, J.; Topf, M.; Rosenfeld, S.S.; et al. The divergent mitotic kinesin MKLP2 exhibits atypical structure and mechanochemistry. *eLife* **2017**, *6*, e27793. [[CrossRef](#)]

77. Adriaans, I.E.; Hooikaas, P.J.; Aher, A.; Vromans, M.J.M.; van Es, R.M.; Grigoriev, I.; Akhmanova, A.; Lens, S.M.A. MKLP2 Is a Motile Kinesin that Transports the Chromosomal Passenger Complex during Anaphase. *Curr. Biol.* **2020**, *30*, 2628–2637. [[CrossRef](#)]
78. Kapitein, L.C.; Peterman, E.J.; Kwok, B.H.; Kim, J.H.; Kapoor, T.M.; Schmidt, C.F. The bipolar mitotic kinesin Eg5 moves on both microtubules that it crosslinks. *Nature* **2005**, *435*, 114–118. [[CrossRef](#)]
79. Van den Wildenberg, S.M.; Tao, L.; Kapitein, L.C.; Schmidt, C.F.; Scholey, J.M.; Peterman, E.J. The homotetrameric kinesin-5 KLP61F preferentially crosslinks microtubules into antiparallel orientations. *Curr. Biol.* **2008**, *18*, 1860–1864. [[CrossRef](#)]
80. Roostalu, J.; Hentrich, C.; Bieling, P.; Telley, I.A.; Schiebel, E.; Surrey, T. Directional switching of the kinesin cin8 through motor coupling. *Science* **2011**, *332*, 94–99. [[CrossRef](#)]
81. Gerson-Gurwitz, A.; Thiede, C.; Movshovich, N.; Fridman, V.; Podolskaya, M.; Danieli, T.; Lakamper, S.; Klopfenstein, D.R.; Schmidt, C.F.; Gheber, L. Directionality of individual kinesin-5 Cin8 motors is modulated by loop 8, ionic strength and microtubule geometry. *EMBO J.* **2011**, *30*, 4942–4954. [[CrossRef](#)] [[PubMed](#)]
82. Fridman, V.; Gerson-Gurwitz, A.; Shapira, O.; Movshovich, N.; Lakamper, S.; Schmidt, C.F.; Gheber, L. Kinesin-5 Kip1 is a bi-directional motor that stabilizes microtubules and tracks their plus-ends in vivo. *J. Cell Sci.* **2013**, *126*, 4147–4159. [[CrossRef](#)] [[PubMed](#)]
83. Edamatsu, M. Bidirectional motility of the fission yeast kinesin-5, Cut7. *Biochem. Biophys. Res. Commun.* **2014**, *446*, 231–234. [[CrossRef](#)] [[PubMed](#)]
84. Singh, S.K.; Pandey, H.; Al-Bassam, J.; Gheber, L. Bidirectional motility of kinesin-5 motor proteins: Structural determinants, cumulative functions and physiological roles. *Cell. Mol. Life Sci.* **2018**, *75*, 1757–1771. [[CrossRef](#)] [[PubMed](#)]
85. Britto, M.; Goulet, A.; Rizvi, S.; von Loeffelholz, O.; Moores, C.A.; Cross, R.A. *Schizosaccharomyces pombe* kinesin-5 switches direction using a steric blocking mechanism. *Proc. Natl Acad. Sci. USA* **2016**, *113*, E7483–E7489. [[CrossRef](#)]
86. Goldstein-Levitin, A.; Pandey, H.; Allhuzaeel, K.; Kass, I.; Gheber, L. Intracellular functions and motile properties of bi-directional kinesin-5 Cin8 are regulated by neck linker docking. *eLife* **2021**, *10*, e71036. [[CrossRef](#)] [[PubMed](#)]
87. Xie, P. A common ATP-dependent stepping model for kinesin-5 and kinesin-1: Mechanism of bi-directionality of kinesin-5. *Biophys. Chem.* **2021**, *271*, 106548. [[CrossRef](#)]
88. Liu, Y.; Wang, Y.; Wang, P.; Xie, P. Effect of kinesin-5 tail domain on motor dynamics for antiparallel microtubule sliding. *Int. J. Mol. Sci.* **2021**, *22*, 7857. [[CrossRef](#)]

Disclaimer/Publisher’s Note: The statements, opinions and data contained in all publications are solely those of the individual author(s) and contributor(s) and not of MDPI and/or the editor(s). MDPI and/or the editor(s) disclaim responsibility for any injury to people or property resulting from any ideas, methods, instructions or products referred to in the content.